Electronic Supplementary Information

Mesomeric control of the optoelectronic properties of polymerized small molecule acceptors

Diego Sorbelli,[a] Yilei Wu[b], Zhenan Bao[b] and Giulia Galli*[acd]

[a] *Pritzker School of Molecular Engineering, University of Chicago, Chicago, IL 60637, USA.*
E-mail: gagalli@uchicago.edu
[b]Department of Chemical Engineering, Stanford University, Stanford, CA, 94305-4125, USA
[c] *Materials Science Division and Center for Molecular Engineering, Argonne National Laboratory, Lemont, IL 60439, USA*
[d] *Department of Chemistry, University of Chicago, Chicago, IL 60637, USA*

Index of contents

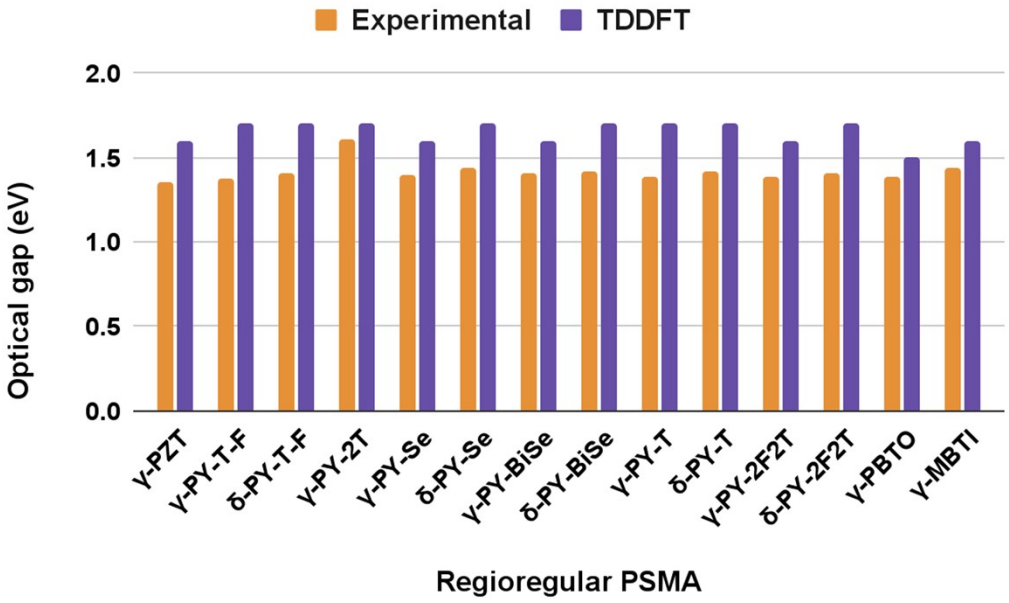

Figure S1. Comparison of the optical gaps of several regioregular PSMAs computed with TDDFT (purple bars) with optical gaps derived from absorption onsets of previously reported experimental UV-Vis spectra (orange bars) from Refs. 1-7

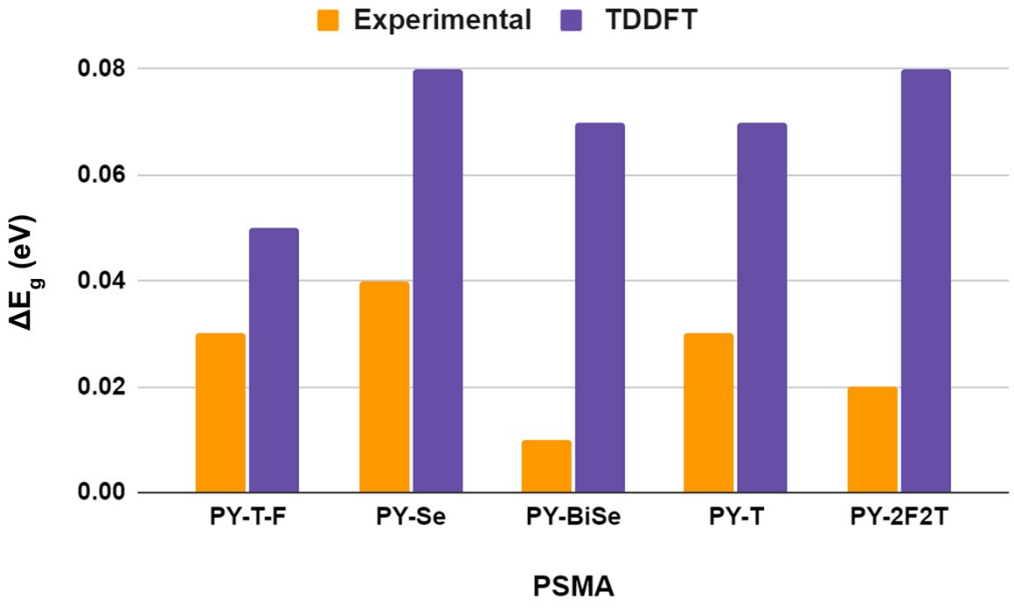

Figure S2. Comparison of the ΔE_g values of several regioregular PSMAs computed with TDDFT (purple bars) with ΔE_g values derived from UV-Vis experiments (orange bars) from Refs. 2-5

Non-empirical gap tuning procedure for long-range corrected hybrid functionals

The range separation parameter (ω) of any long-range corrected functional can be optimized for each system of interest separately following a non-empirical gap-tuning procedure.[8-10] This procedure is aimed at adjusting the value of ω to fulfill a fundamental property that an exact exchange-correlation functional must obey in exact Kohn-Sham theory: for an N-electron system, the negative of the HOMO energy *(-ε_{HOMO})* must be equal to the vertical ionization potential (*IP(N)*). Considering that PSMAs are donor-acceptor system, it is common to focus on the vertical electron affinity as well, which can be considered as the ionization potential of the N+1 electron system (*IP(N+1)*).[10-11]
The vertical ionization potentials can be defined as follows:

$$IP(N) = E_0(N-1) - E_0(N) \quad (S1)$$

$$IP(N+1) = E_0(N) - E_0(N+1) \quad (S2).$$

In this context, the optimal ω value is the one that minimizes the following expression:

$$J^2(\omega) = \left[\varepsilon_{HOMO}^{\omega}(N) + IP^{\omega}(N)\right] + \left[\varepsilon_{HOMO}^{\omega}(N+1) + IP^{\omega}(N+1)\right] \quad (S3)$$

where $\varepsilon_{HOMO}^{\omega}(N)$ and $\varepsilon_{HOMO}^{\omega}(N+1)$ are the energies of the HOMO of the neutral and anion states of the system. Alternatively, it has been shown that a similar procedure can be carried out using LUMO energies as follows:[8-11]

$$J^2(\omega) = \left[\varepsilon_{HOMO}^{\omega}(N) + IP^{\omega}(N)\right] + \left[\varepsilon_{LUMO}^{\omega}(N) + IP^{\omega}(N+1)\right] \quad (S4)$$

where $\varepsilon_{HOMO}^{\omega}(N)$ and $\varepsilon_{LUMO}^{\omega}(N)$ are the energies of the LUMO of the neutral state of the system.

The expression in Eq. S4 is the one used in this work. The optimal range-separation parameter (ω*) for IC- and IND-terminated δ- and γ-PY-2T dimers are reported in Table S1.

PSMA	ω* (a_0^{-1})
γ-PY-2T	0.0982
δ-PY-2T	0.0980
γ-PY-2T-IND	0.1072
δ-PY-2T-IND	0.1085

Table S1. Optimal values of the range-separation parameter (ω*) for IC- and IND-terminated δ- and γ-PY-2T derived from the non-empirical gap tuning procedure using the ωB97XD long-range corrected hybrid functional.

γ-PY-2T				
XC functional	**E_{HL} (eV)**	**E_g (eV)**	**E_b (eV)**	**p (%)**
B3LYP	1.95	1.68	0.27	6.7
ω*B97XD	3.89	1.97	1.90	5.3
Experimental	1.93	1.63	/	/
δ-PY-2T				
XC functional	**E_{HL} (eV)**	**E_g (eV)**	**E_b (eV)**	**p (%)**
B3LYP	1.97	1.72	0.25	0.6
ω*B97XD	3.89	1.98	1.91	0.4
γ-PY-2T-IND				
XC functional	**E_{HL} (eV)**	**E_g (eV)**	**E_b (eV)**	**p (%)**
B3LYP	2.17	1.93	0.25	4.6
ω*B97XD	4.35	2.24	2.07	4.2
δ-PY-2T-IND				
XC functional	**E_{HL} (eV)**	**E_g (eV)**	**E_b (eV)**	**p (%)**
B3LYP	2.17	1.92	0.25	4.4
ω*B97XD	4.30	2.23	4.29	4.0

Table S2. HOMO-LUMO gaps (E_{HL}), optical gaps (E_g), exciton binding energies (E_b) and linker reduced LUMO populations (p) computed with B3LYP and with the gap-tuned ω*B97XD functional for IC- and IND-terminated δ- and γ-PY-2T. Experimentally derived E_{HL} and E_g from Ref. 3 are reported for γ-PY-2T for comparison.

XC functional/basis set	E_{HL} (eV)	E_g (eV)	E_b (eV)
B3LYP/def2-SVP	1.98	1.71	0.27
B3LYP/def2-TZVPP	1.95	1.68	0.27
ω*B97XD/def2-SVP	3.89	1.97	1.90
ω*B97XD/def2-TZVPP	3.75	1.90	1.85
Experimental	1.93	1.63	/

Table S3. Basis set effect on the HOMO-LUMO gap (E_{HL}), optical gap (E_g) and exciton binding energy (E_b) computed with the B3LYP and with the gap-tuned ω*B97XD functional for the γ-PY-2T polymer. The optimal ω value for γ-PY-2T computed with the def2-SVP and def2-TZVPP basis sets is 0.0982 and 0.0922 a_0^{-1}, respectively. Experimentally derived E_{HL} and E_g from Ref. 3 are reported for comparison.

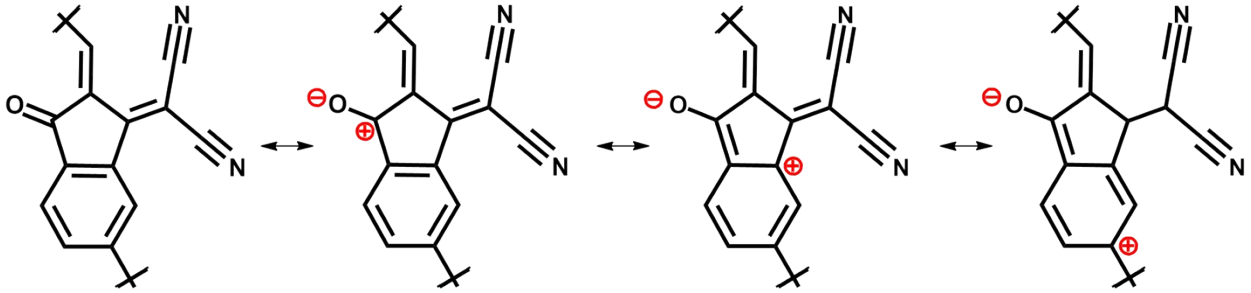

Scheme S1. Lewis resonance structures representing the negative mesomeric effect induced by the keto substituent on the IC unit of δ-PSMAs.

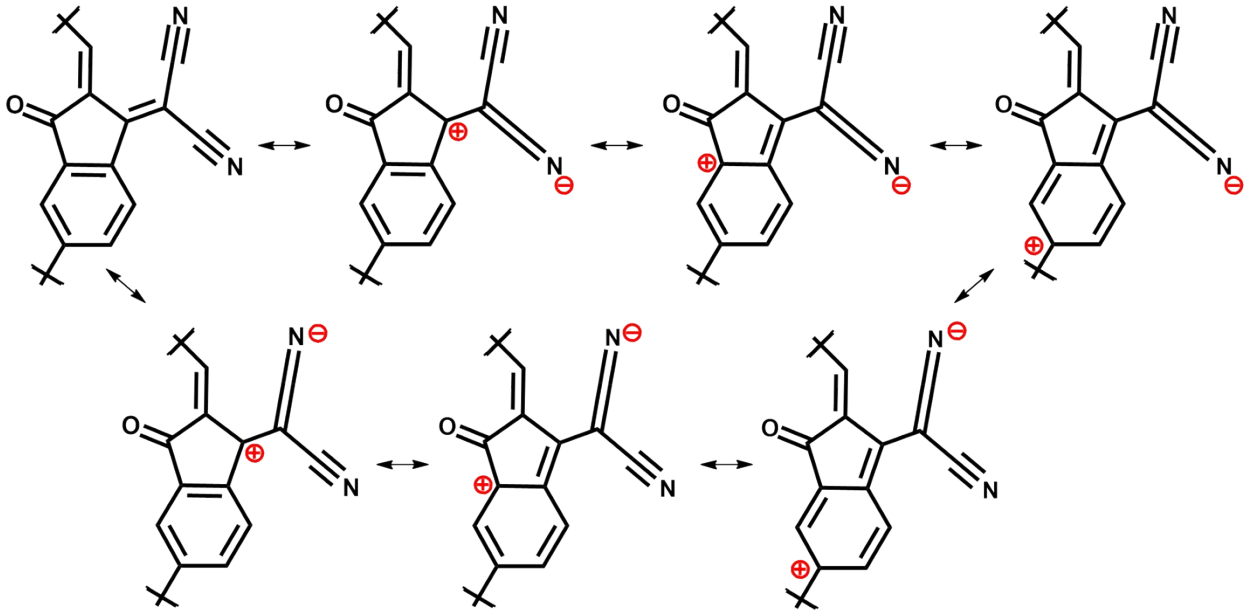

Scheme S2. Lewis resonance structures representing the negative mesomeric effect induced by the dicyanomethylene substituent on the IC unit of γ-PSMAs.

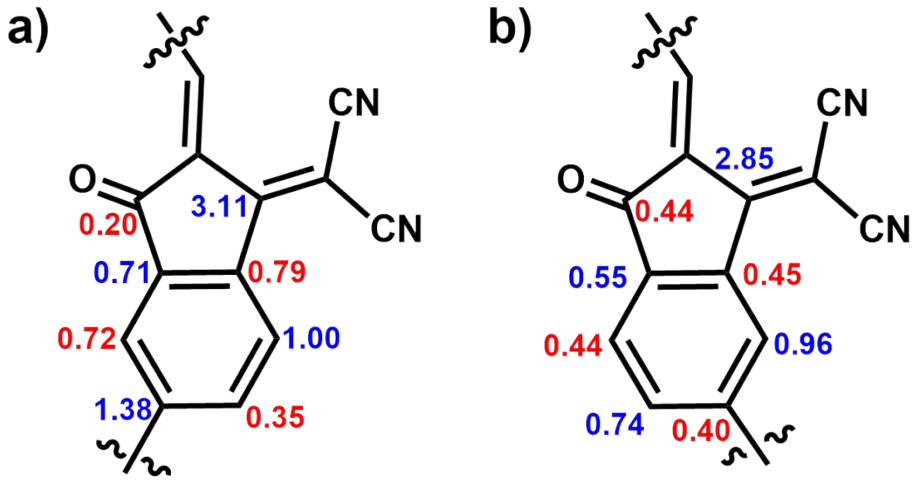

Figure S3. Schematic structure of the IC unit of γ- (a) and δ-PY-2T (b) together with the reduced atomic LUMO populations (in percentage) on the carbon atoms of the IC unit. The values in blue (red) represent the positions of the IC unit where the formal positive charge delocalizes along the γ (δ) conjugation pattern according to the resonance structures in Schemes S1 and S2.

The reduced atomic LUMO populations on the IC units of γ- (Figure S3a) and δ-PY-2T (Figure S3b), and the delocalization of the LUMOs of the two isomers over the IC units, reflect the resonance structures reported in Schemes S1 and S2 and, therefore, the different mesomeric effects along the two conjugation patterns. According to Scheme S1, due to the mesomeric effects associated to the keto group, a formal positive charge is delocalized on the ipso position (i.e. where the keto group is attached), and on the β, δ, and ζ positions of the phenyl ring of the IC unit (see Scheme S1 or red labels in Figure S3). According to Scheme S2, due to the stronger mesomeric effects associated to the dicyanomethylene group, two formal positive charges delocalize on the ipso position (i.e. where the dicyanomethylene group is attached), and on the α, γ, and ε positions of the phenyl group (see Scheme S2 or blue labels in Figure S3). The LUMO, an empty orbital, formally follows these patterns, by delocalizing on the atoms of the IC unit that bear the highest formal positive charge. The data in Figure S3 show that indeed this is the case for PY-2T: for both isomers, the LUMO is comparatively more localized on the positions controlled by the mesomeric effects of the dicyanomethylene group (blue labels) compared to the ones controlled by the keto group (red labels), indicating that mesomeric effects are directly related to the pattern followed by the LUMO delocalization on the IC unit.

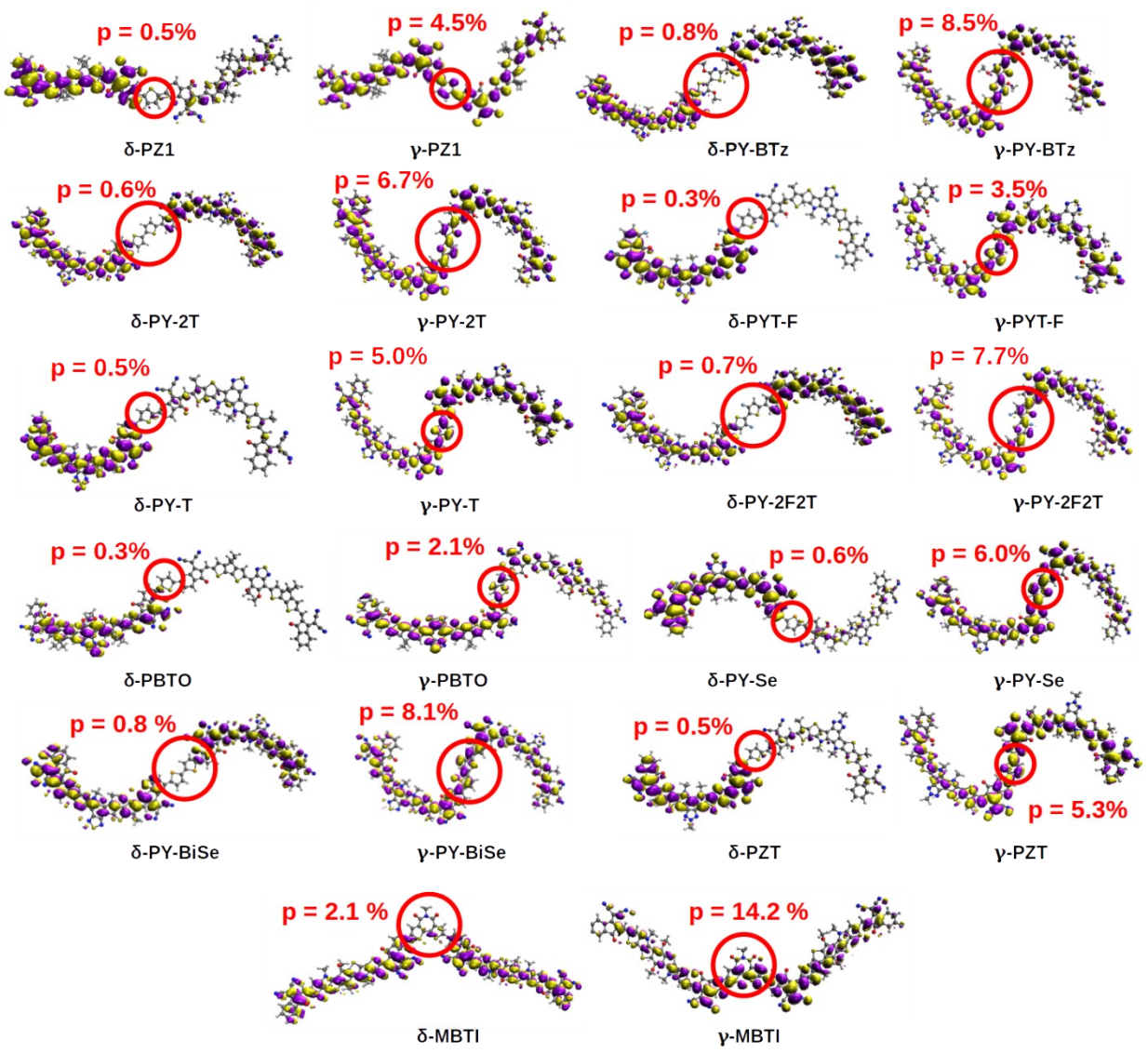

Figure S4. LUMO isosurfaces (isodensity value 10 me/a_0^3) for the δ and γ isomers of all IC-terminated PSMAs under study in this work. For each isosurface, the percentage of LUMO localization on the linker unit (*p*) is reported.

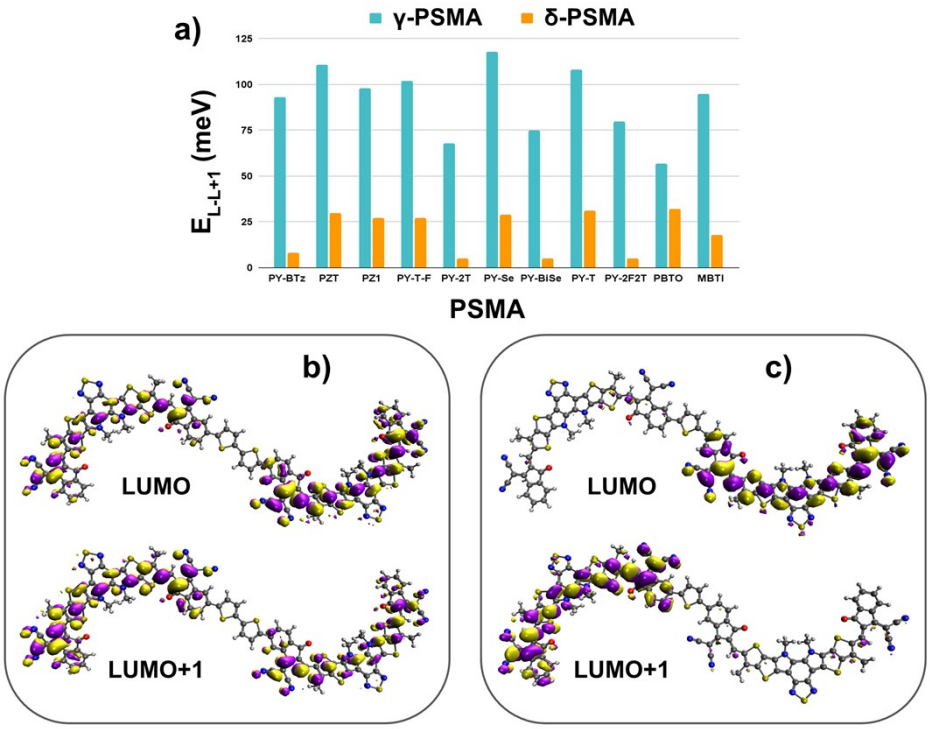

Figure S5. a) Values of the LUMO-LUMO+1 gaps (E_{L-L+1}) for all the γ- (light blue) and δ-PSMAs (orange) studied here. b) The isosurfaces of LUMO and LUMO+1 (isodensity value 10 me/a_0^3) for δ-PY-2T. c) The isosurfaces of LUMO and LUMO+1 (isodensity value 10 me/a_0^3) for δ-PY-T.

Inspection of the LUMO isosurfaces in Figure S4 reveals that different delocalization patterns are observed among different δ-PSMAs. We find that δ-PSMAs bearing single-unit π-linkers like thiophenes and selenophenes (i.e. δ-PY-T, δ-PYT-F, δ-PBTO, δ-PZT, δ-PY-Se) display LUMOs that are only localized on one of the SMA units. On the other hand, in δ-PSMAs bearing double-unit π-linkers like bithiophene, biselenophene, bithiazole (i.e. δ-PY-2T, δ-PY-2F2T, δ-MBTI, δ-PY-BTz, δ-PY-BiSe), the LUMO is localized on both SMA units but not on the π-linker. These differences among δ-PSMAs can be explained by inspecting the energy and shape of the LUMO+1 levels: as shown in Figure S5a, the LUMO-LUMO+1 energy difference is very small (on average 19 ± 11 meV), indicating an orbital quasi-degeneracy. Furthermore, comparing the isosurfaces of PY-T and PY-2T as representative examples, we see that for PY-T (single-unit linker, Figure S5c), the LUMO is localized on one repeating unit, whereas the LUMO+1 is localized on the other SMA unit. For PY-2T (double-unit linker, Figure S5c), the LUMO +1, similarly to the LUMO, is localized on both SMA units, but displays opposite orbital phase signs compared to the LUMO on one of the SMA units (right SMA unit in Figure S5b). These features indicate that it is appropriate to consider a linear combination of the LUMO and the LUMO+1 in all cases; this linear combination indicates that the different orbital localization features mostly arise from the symmetry of the π-linker, rather than from actual differences in the delocalization patterns. Notably, we find that in all cases no LUMO localization is found on the π-linkers of δ-PSMAs, consistent with our analysis on the LUMO delocalization based on p values.

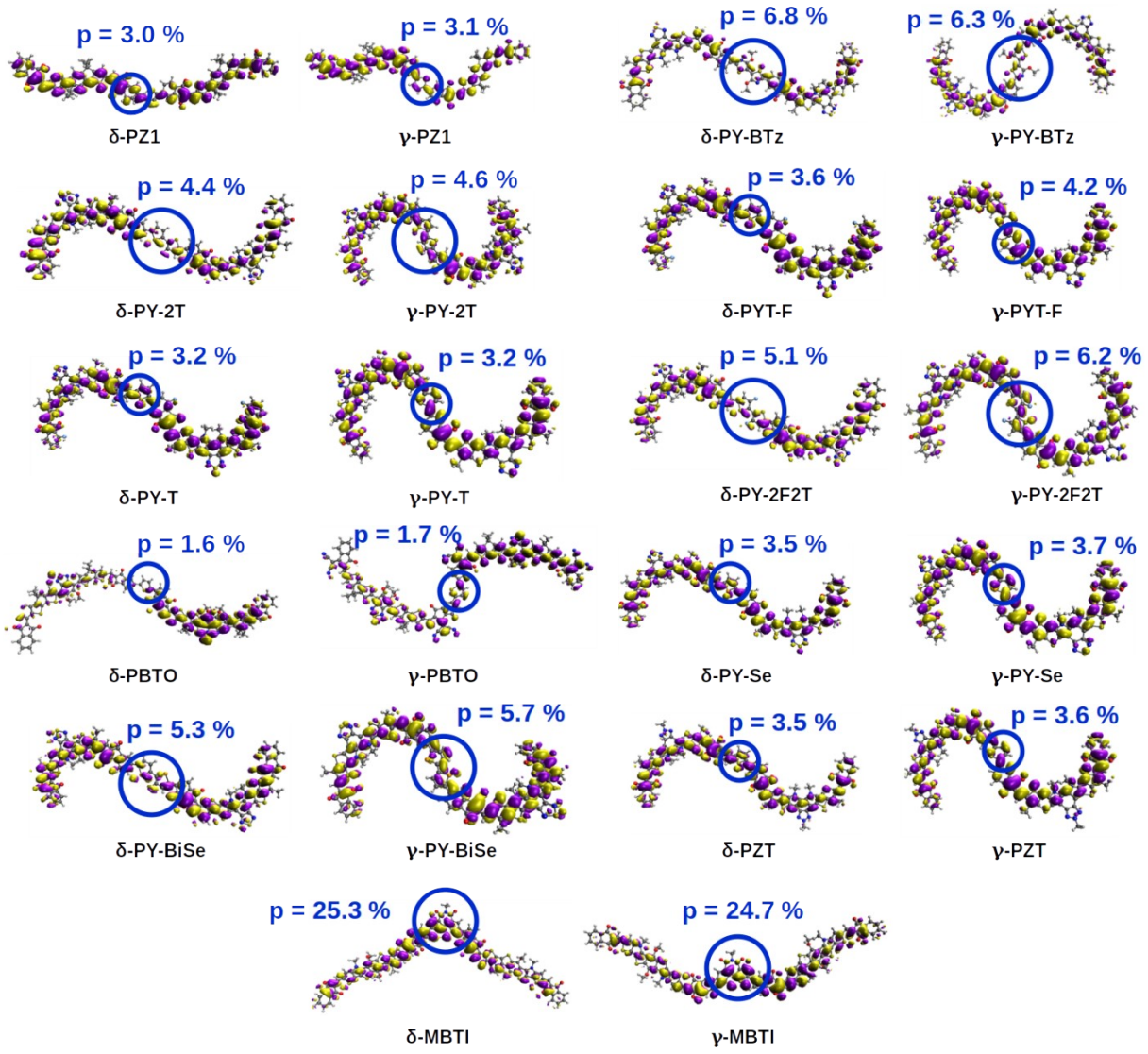

Figure S6. LUMO isosurfaces (isodensity value 10 me/a_0^3) for the δ and γ isomers of all IND-terminated PSMAs under study in this work. For each isosurface, the percentage of LUMO localization on the linker unit (*p*) is reported.

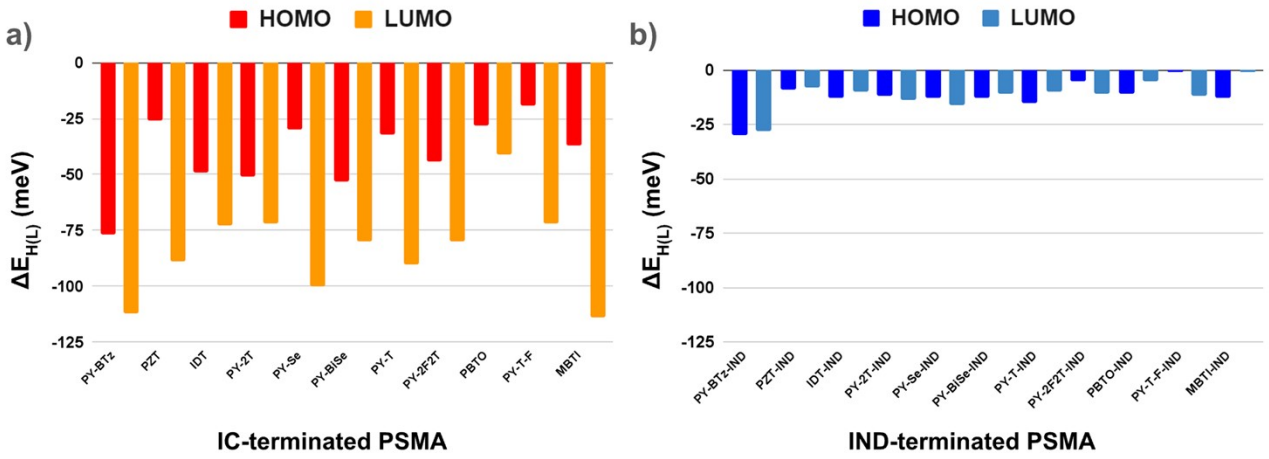

Figure S7. Regioregularity effect on HOMO (ΔE_H) and LUMO (ΔE_L) energies for IC- (a) and IND-terminated (b) PSMAs, where both are defined as: $\Delta E_{H(L)} = E_{H(L)}^{\gamma} - E_{H(L)}^{\delta}$.

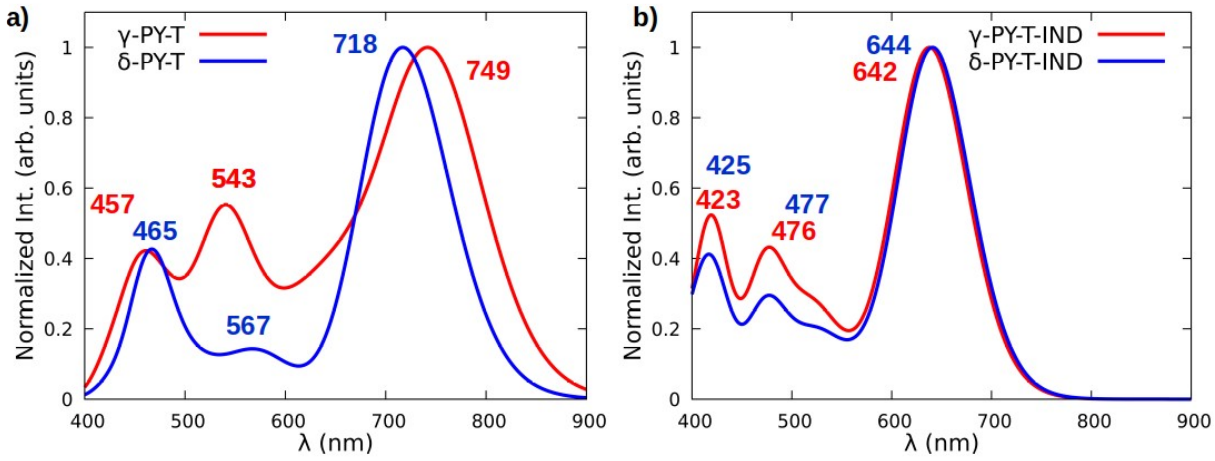

Figure S8. Computed absorption spectra for δ- and γ-PY-T (a) and δ- and γ-PY-T-IND (b). The wavelengths (in nm) associated to the main absorption peaks are shown on the top of each peak.

The main features of the absorption spectra of the different isomers of PY-T, taken as a representative example, are reported in Figure S8. As shown in Figure S8a, the computed absorption spectra of δ- and γ-PY-T are in qualitative agreement: they are both characterized by a low-energy (700-750 nm) main absorption peak associated to the bright S_1 state (associated to the HOMO -> LUMO single-particle transition). Additionally, we find two higher-energy peaks for both isomers: one around 550 nm, mainly associated to a HOMO-2-to-LUMO transition and another one around 450 nm, mainly associated to a HOMO-5-to-LUMO+1 transition. The spectra of δ- and γ-PY-T-IND (Figure S8b) display similar absorption peaks arising from analogous single-particle transitions (i.e. a HOMO-to-LUMO transition for the lowest energy peak, a HOMO-2-to-LUMO transition for the peak around 470 nm and an HOMO-5-to-LUMO transition for the highest-energy absorption peak). The only noticeable differences are the relative positions of the peaks. In particular, the spectra in Figure S8a clearly show that the dominant low-lying absorption peak of γ-PY-T (749 nm) is red-shifted compared to that of δ-PY-T (718 nm), while δ- and γ-PY-T-IND exhibit nearly overlapping peaks (Figure S8b). These results indicate that the nature of the excited states of these isomers is mostly controlled by the inherent chemical structure of the monomeric unit, and it is therefore not remarkably influenced by regioregularity. On the other hand, the energy of the states (particularly of the bright low-lying S_1 state) is controlled by regioregularity, specifically by the enhanced conjugation length and mesomeric effects at the γ site.

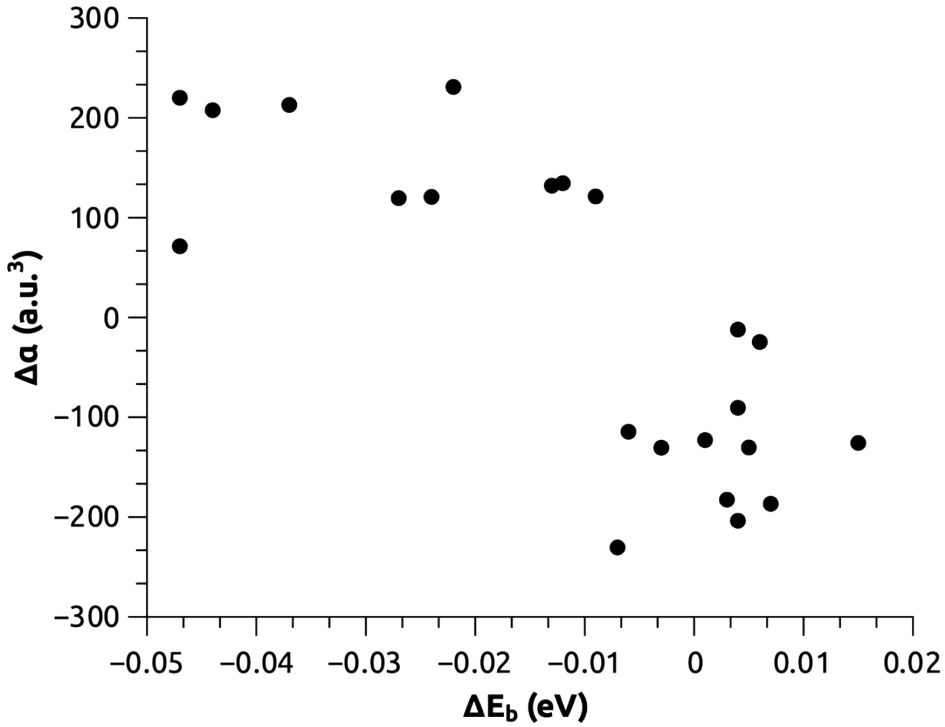

Figure S9. Plot between the regioisomer effect on exciton binding energies ($^{\Delta E_b}$) and the regioisomer effect on isotropic polarizability ($^{\Delta\alpha}$, defined as: $\Delta\alpha = \alpha^{\delta} - \alpha^{\gamma}$) for IC- and IND-terminated PSMAs.

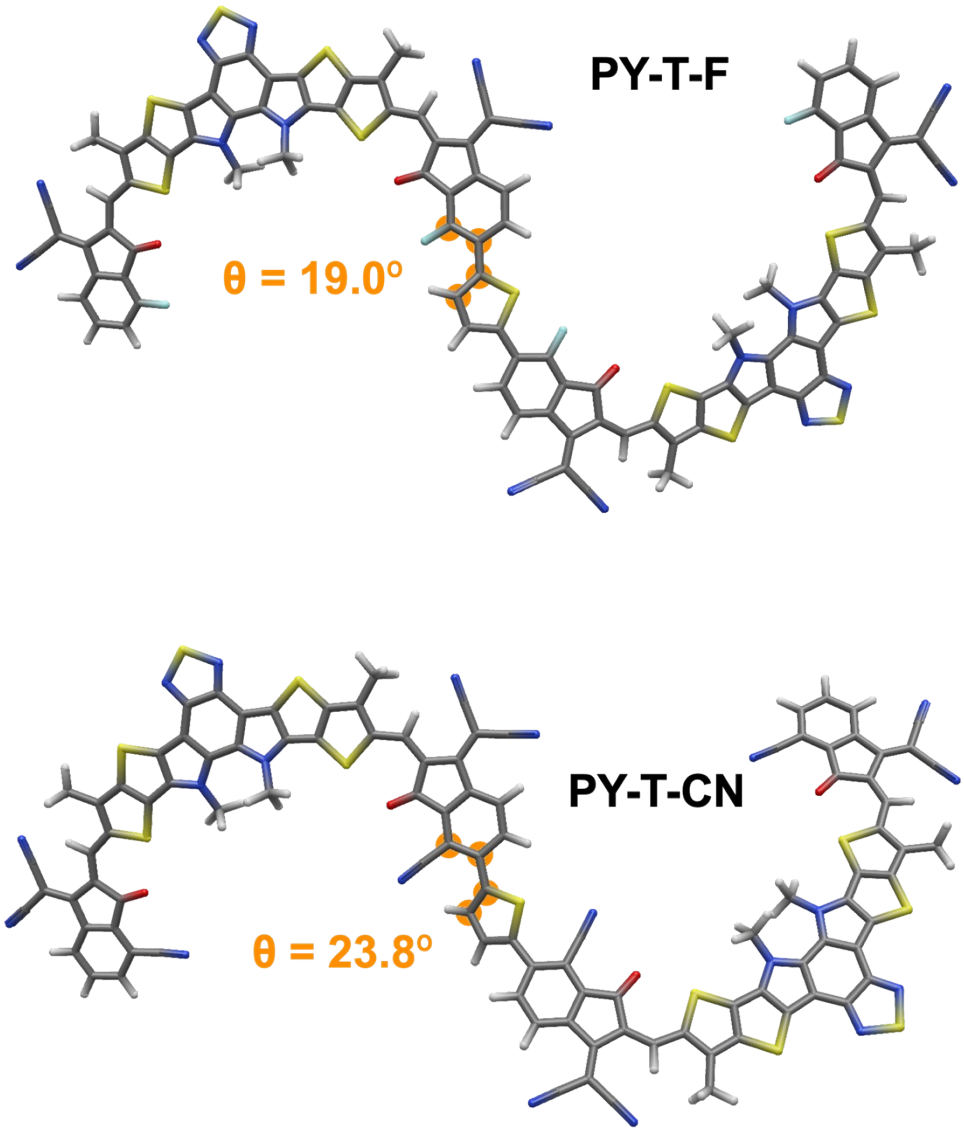

Figure S10. Optimized ground state structures of γ-PY-T-F (top) and γ-PY-T-CN (bottom) dimers. The linker-SMA dihedral angles is reported for both.

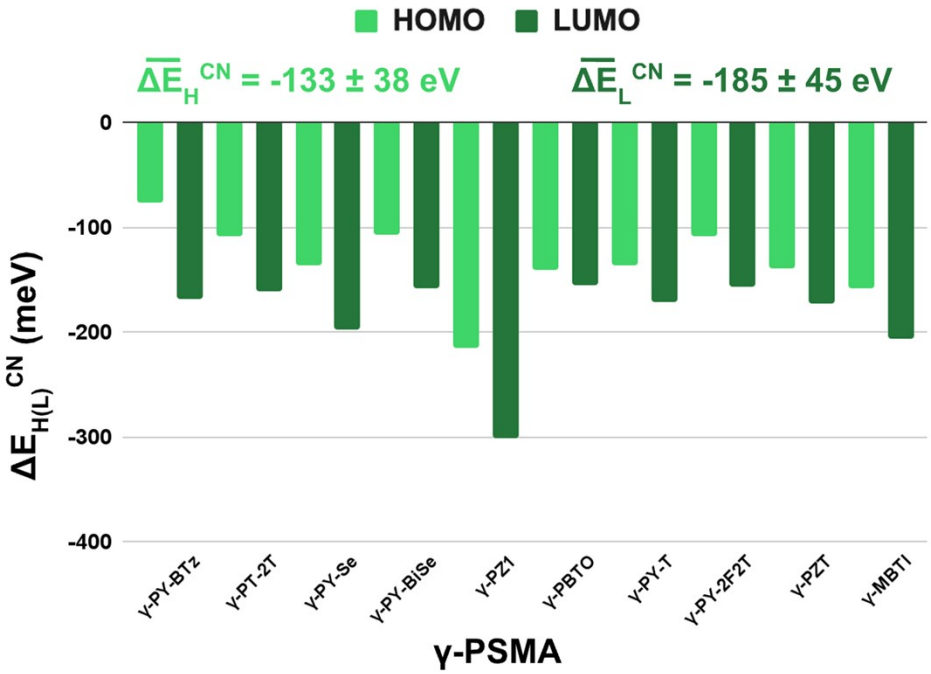

Figure S11. Effect of cyano-functionalization at the β position of the IC unit of γ-PSMAs on HOMO (light green bars) and LUMO (dark green bars) energies, defined as: $\Delta E_{H(L)}^{CN} = E_{H(L)}^{\gamma-CN} - E_{H(L)}^{\gamma}$. The average value of each property is reported.

References

1 H. Fu, Y. Li, J. Yu, Z. Wu, Q. Fan, F. Lin, H. Y. Woo, F. Gao, Z. Zhu and A. K. Y. Jen, *J. Am. Chem. Soc.*, 2021, **143**, 2665–2670

2 H. Yu, M. Pan, R. Sun, I. Agunawela, J. Zhang, Y. Li, Z. Qi, H. Han, X. Zou, W. Zhou, S. Chen, J. Y. L. Lai, S. Luo, Z. Luo, D. Zhao, X. Lu, H. Ade, F. Huang, J. Min and H. Yan, *Angew. Chem. Int. Ed.*, 2021, **60**, 10137–10146.

3 H. Wang, H. Chen, W. Xie, H. Lai, T. Zhao, Y. Zhu, L. Chen, C. Ke, N. Zheng and F. He, *Adv. Funct. Mater.*, 2021, **31**, 2100877.

4 S. Seo, C. Sun, J.-W. Lee, S. Lee, D. Lee, C. Wang, T. Ngoc-Lan Phan, G.-U. Kim, S. Cho, Y.-H. Kim, B. J. Kim, S. Seo, J. Lee, S. Lee, T. N-L Phan, G. Kim, B. J. Kim, C. Sun, Y. Kim, D. Lee, S. Cho and C. Wang, *Adv. Funct. Mater.*, 2022, **32**, 2108508.

5 Z. Luo, T. Liu, R. Ma, Y. Xiao, L. Zhan, G. Zhang, H. Sun, F. Ni, G. Chai, J. Wang, C. Zhong, Y. Zou, X. Guo, X. Lu, H. Chen, H. Yan and C. Yang, *Adv. Mater.*, 2020, **32**, 2005942.

6 C. Wang, J. Fang, C. Guan, T. Wu, X. Liu, F. Liu, C. Xiao and W. Li, *ACS Appl. Mater. Interfaces*, 2023, **15**, 13363–13370.

7 H. Sun, B. Liu, Y. Ma, J.-W. Lee, J. Yang, J. Wang, Y. Li, B. Li, K. Feng, Y. Shi, B. Zhang, D. Han, H. Meng, L. Niu, B. J. Kim, Q. Zheng and X. Guo, *Adv. Mater.*, 2021, **33**, 2102635.

8 T. Stein, H. Eisenberg, L. Kronik and R. Baer, *Phys. Rev. Lett.*, 2010, **105**, 266802.

9 N. Kuritz, T. Stein, R. Baer and L. Kronik, *J. Chem. Theory Comput.*, 2011, **7**, 2408–2415.

10 L. Kronik, T. Stein, S. Refaely-Abramson and R. Baer, *J. Chem. Theory Comput.* 2012, **8**, 1515–1531.

11 H. Sun, C. Zhong and J. L. Brédas, *J. Chem. Theory Comput.* 2015, **11**, 3851–3858.